# Anatomy of an Energy-Coupling Mechanism—The Interlocking Catalytic Cycles of the ATP Sulfurylase−GTPase System†

Meihao Sun and Thomas S. Leyh*

*The Department of Biochemistry, Albert Einstein College of Medicine, 1300 Morris Park Avenue, Bronx, New York 10461-1926*

*Received July 7, 2005; Revised Manuscript Received August 26, 2005*

ABSTRACT: ATP sulfurylase, from *Escherichia coli K*-12, conformationally couples the rates and chemical potentials of the two reactions that it catalyzes, GTP hydrolysis and activated sulfate synthesis. The enzyme is rare among such coupling systems in that it links the potentials of small-molecule chemistries to one another, rather than to vectorial motion. The pre-steady-state stages of the catalytic cycle of ATP sulfurylase were studied using tools capable of distinguishing between enzyme-bound and solution-phase product for each of the four products of the enzyme. The study reveals that the two chemistries are linked at multiple points in the reaction coordinate. Linking begins with an isomerization prior to chemistry that initiates an ordered cleavage of the $\beta,\gamma$ and $\alpha,\beta$ bonds of GTP and ATP, respectively; the rates of these three sequential events increase successively, causing them to appear simultaneous. Linking is again seen in the late stages of the catalytic cycle: product release is ordered with $P_i$ departing prior to either GDP or $PP_i$. Release rate constants are determined for each product and used to construct a quantitative model of the mechanism that accurately predicts the behavior of this complex system.

Sulfur, essential to life as we know it, is found in hundreds of metabolites across multiple oxidation states (*1*−*4*). Sulfate, a primary sulfur nutrient, is a stable nonreactive compound that is chemically activated *in vivo* by enzymatic transfer of the adenylyl (∼AMP) moiety of ATP to form the high-energy phosphoric−sulfuric acid anhydride bond that is the hallmark of activated sulfate [adenosine 5′-phosphosulfate or APS (*5*, *6*)]. From its activated state, the sulfuryl moiety ($\sim SO_3^-$) of APS is poised for facile and favorable entry into its metabolic fates of sulfuryl transfer [used to regulate metabolism (*7*−*9*)] and reduction [used for the biosynthesis of reduced-sulfur metabolites and as an electron sink for the electron-transport chain (*1*, *10*)].

The activating chemistry is catalyzed by ATP sulfurylase (ATP:sulfate adenylyltransferase, EC 2.7.7.4), which, in *Escherichia coli K*-12, is a tetramer of heterodimers each composed of an adenylyl transferase (CysD, 35 kDa) and a GTPase (CysN, 53 kDa) (*11*, *12*). ATP sulfuryase is remarkable in that it is capable of conformationally coupling the chemical potentials of the two small-molecule chemistries that it catalyzes (*13*, *14*), GTP hydrolysis and activated sulfate synthesis, reactions 1 and 2.

$$ATP^{-4} + SO_4^{-2} \leftrightarrows APS^{-2} + P_2O_7^{-4} \quad (1)$$

$$GTP^{-4} + H_2O \leftrightarrows GDP^{-3} + HPO_4^{-2} + H^+ \quad (2)$$

The potential of the phosphoric−sulfuric acid anhydride bond found in APS is extremely high ($\Delta G'_{0\ \mathrm{hydrolysis}} \sim -19$ kcal/mol); consequently, its synthesis from ATP and $SO_4$, under presumed physiological conditions, is quite unfavorable, $K_{eq} \sim 10^{-8}$ (*4*, *6*, *15*). This large thermodynamic bias results in a kinetic consequence that cannot be circumvented by coupling the Gibbs potentials of favorable downstream metabolic chemistries, which is that the catalytic efficiency of the enzyme must be $\sim 10^{-8}$ less favorable, in this case, in the physiological direction (*16*). Inefficiencies of this magnitude place catalysts at risk of being incapable of providing adequate, timely supplies of their nutrients to the cell. Overcoming such inefficiencies requires that a relatively favorable chemistry (e.g., GTP hydrolysis) be physically linked to the catalyst such that the steps of its chemistry can be harnessed to those of the less favorable reaction and thereby used to drive the catalyst through its cycle. Such is the case with ATP sulfurylase. How and where this coupling occurs in the catalytic cycle is the central focus of this paper.

## MATERIALS AND METHODS

The materials and suppliers used in this study are as follows: [$\gamma$-$^{32}$P]ATP, [$\gamma$-$^{32}$P]GTP, and [$\alpha$-$^{32}$P]GTP (Perkin−Elmer Life Science Products), [$^{35}$S]$Na_2SO_4$ (ICN Pharmaceuticals), sephadex G-25 gel-filtration resin (Sigma), 7-(diethylamino)-3-((((2-male-imidyl)ethyl)amino)carbonyl)-coumarin (MDCC) (Molecular Probes), Q-sepharose fast flow and Superdex 200 prep-grade resins (Pharmacia), competent BL21 (DE3) and His·Bind resin (Novagen), and poly-(ethylenimine)-cellulose-F thin-layer chromatography plates (TLC plates) (EM Science). The other reagents and salts were the highest grades available from Sigma or Fisher.

*Coupling Enzymes.* Inorganic pyrophosphatase ($PP_i$ase, rabbit muscle), lactate dehydrogenase (LDH, rabbit muscle), and pyruvate kinase (PK, rabbit muscle) were purchased from Roche Diagnostics. The enzymes were dialyzed extensively

† Supported by the National Institutes of Health Grant GM54469.

* To whom correspondence should be addressed: The Department of Biochemistry, Albert Einstein College of Medicine, 1300 Morris Park Ave., Bronx, NY 10461-1926. Telephone: 718-430-2857. Fax: 718-430-8565. E-mail: leyh@aecom.yu.edu.

10.1021/bi051303e CCC: $30.25 © 2005 American Chemical Society
Published on Web 10/01/2005

against 50 mM *N*-2-hydroxyethylpiperazine-*N*′−2-ethanesulfonic acid (Hepes)[1]/KOH (pH 8.0) before using. APS kinase, from yeast, was expressed in *E. coli* and purified as describe previously (*17*). Phosphate-binding protein [PBP, (A197C)-MDCC ] was expressed, purified, and labeled with MDCC as described previously (*18*, *19*).

*ATP Sulfurylase.* The enzyme, from *E. coli*, was expressed in *E. coli*, purified, and stored as described previously (*20*).

*Quenched-Flow Experiments.* Experiments were performed with a Kin-Tek quench-flow apparatus, model RQF-3. Reactions were quenched with EDTA/NaOH (100 mM, pH 10) and boiled for 1 min, and the radiolabeled reactants and products were then separated on PEI-F TLC (*21*) sheets using the following mobile phases: 0.90 M LiCl was used to separate APS from sulfate and phosphate from GTP or ATP; GTP and GDP were separated using either 0.75 M Tris and 0.45 M HCl [Tb buffer (*22*)] or 0.5 M LiCl; and ATP, $PP_i$, and phosphate were separated using a two-dimensional separation: 0.9 M LiCl (dimension one) and 1.2 M triethylamine/$HCO_3^-$ at pH 7.4 (dimension two). Radiolabeled reactants were quantitated using a Molecular Dynamics, Storm 820, 2D-imaging system.

*Stopped-Flow Experiments.* The formation of solution-phase GDP and phosphate was monitored using a stopped-flow spectrofluorimeter (Applied Photophysics SX-18MV). Phosphate-detection experiments, which used PBP, used a 425 nm excitation wavelength and a 455 nm cutoff filter (which allows detection above ~455 nm). Successful use of the PBP system requires that $P_i$ be removed scrupulously from all solutions and surfaces (including the syringes and mixing chamber) associated with the experiment. This is accomplished using an enzymatic coupling system [purine nucleoside phosphorylase (PNP) and 7-methylguanosine] that removes $P_i$ (*18*, *19*). GDP-detection experiments, which used PK and LDH, used a 340 nm excitation wavelength and a 400 nm cutoff filter. Each of the stopped-flow progress curves shown in this paper is an average of five to eight scans. Fluorescence was converted into phosphate or GDP concentrations using standard curves. All solutions and sample lines were equilibrated at 25 ± 2 °C before mixing.

## RESULTS AND DISCUSSION

*Product Bursts.* When ATP sulfurylase is saturated with ATP, GTP, and $SO_4$, it cleaves the α,*β* and *β*,*γ* bonds of the nucleotides in a 1:1 ratio (*23*). Under these "fully coupled" conditions, the chemical potential of GTP hydrolysis is virtually completely coupled to APS synthesis (*23*−*25*). Catalytic coupling of the solution-phase energetics of two chemistries requires that the catalytic cycle contain steps that create an interdependence of the reactions. This is accomplished via allosteric communication that enables event(s) at a given active site to gate event(s) at the distal site. This "gating" is tantamount to an ordering of steps in the cycles with respect to one another. To begin to define where such ordering occurs in the catalytic cycle of ATP sulfurylase, product formation was monitored in the pre-steady-state phase of the catalytic cycle (see Figure 1). The reactions were initiated by rapidly mixing ATP sulfurylase with a solution containing ATP, GTP, and $SO_4$ at saturating concentrations and coupling enzymes [APS kinase, inorganic pyrophosphatase ($PP_i$ase), and pyruvate kinase (PK)] that remove the product, preventing the complications of product-mediated activation of GTP hydrolysis and inhibition (*26*, *27*). GTP hydrolysis and APS synthesis were monitored separately using radiolabeled substrate ([$\gamma$-$^{32}$P]GTP and [$^{35}$S]$SO_4$). The reactions were aged for the time intervals indicated in Figure 1 and quenched by mixing rapidly, 1:1, with ethylenediaminetetraacetic acid (EDTA) (150 mM, pH 10.0). The reactants were separated using thin-layer chromatography and quantitated (see the caption of Figure 1 for further details).

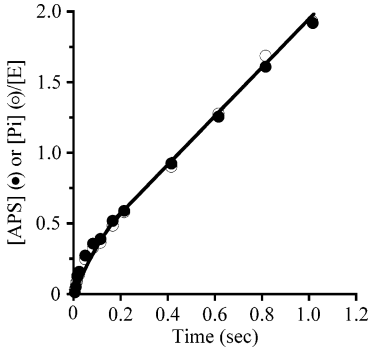


FIGURE 1: Similar pre-steady-state burst in both chemistries. The hydrolysis of GTP. A solution containing [$\gamma$-$^{32}$P]GTP [520 $\mu$M, specific activity (SA) = 38 $\mu$Ci/mL], ATP (1.0 mM), $Na_2SO_4$ (1.0 mM), $MgCl_2$ (3.0 mM), PEP (2.0 mM), APS kinase (106 $\mu$M), $PP_i$ase (53.6 $\mu$M), PK (220 $\mu$M), $MgCl_2$ (6.0 mM), and 50 mM Hepes (pH 8.0) was mixed rapidly using a quenched-flow instrument with a solution of equal volume containing ATP sulfurylase (40 $\mu$M) and 50 mM Hepes (pH 8.0). The mixture was aged for a defined period and quenched by mixing with 150 mM EDTA/NaOH at pH 10.0. The formation of APS. The experimental conditions were identical to those described above, except that GTP (2.0 mM) and [$^{35}$S]$NaSO_4$ (500 $\mu$M, SA = 42 $\mu$Ci/mL) were used. The instrument and solutions were equilibrated at 25 ± 2 °C prior to mixing. Radiolabeled reactants were separated with TLC sheets and quantitated as described in *Materials and Methods*. Each point represents the average of three experiments. The smooth curve is the behavior predicted by the best-fit parameters obtained from a minimal model of the mechanism (see Figure 7 and *Modeling*).

The two reactions exhibit clear, experimentally indistinguishable pre-steady-state bursts of product. Bursts occur because the catalytic cycle contains rate-limiting steps following product formation (*28*). Such steps can be associated with the release itself (i.e., concomitant with release) or can occur before or after release. Because the two overall reactions (hydrolysis and APS synthesis) are coupled in a 1:1 ratio, a rate-determining step in any one of the release "branches" will cause bursts of equal amplitude in both reactions. Thus, any one of the four products of the ATP sulfurylase reaction (not considering protons) can rate-limit the cycle and cause the burst.

Remarkably, the bond-breaking steps of these two very different chemistries appear to be simultaneous. The α,*β*-cleavage reaction is essentially that of a phosphate diester reacting with a poor nucleophile, sulfate, whereas GTP hydrolysis represents a phosphate monoester reacting with what is likely to be activated water. Mono- and diester cleavage reactions are mechanistically distinct. In solution,

[1] Abbreviations: SA, specific activity ($\mu$Ci/mL); EDTA, ethylenediaminetetraacetic acid; Hepes, *N*-2-hydroxyethylpiperazine-*N*′−2-ethanesulfonic acid; PNP, purine nucleoside phosphorylase; U, unit (1 $\mu$mol of product formed/min at saturating substrate).

monoester reactions are dissociative and expected to involve release of the *meta*-phosphate monoanion (*29*, *30*), whereas diester cleavage is a fundamentally associative reaction that proceeds through a pentacoordinate-phosphorus intermediate (*29*, *30*). Under the slightly basic conditions of this experiment, diesters are expected to react orders of magnitude more slowly than comparable monoesters (*31*); however, on the surface of the enzyme, the energetics of the cleavage reactions have been balanced such that they appear to be simultaneous. The cleavages occur at several hundreds per second (see *Modeling*); thus, once the catalytically active form(s) of the active site is assembled, chemistry happens quickly relative to many of the surrounding steps in the catalytic cycle.

The ATP·$SO_4$·E·GMPPNP complex of ATP sulfurylase isomerizes when the last of the three ligands binds to the enzyme (*32*). Single-turnover studies capable of detecting as little as 0.4% of an active-site equivalent of the product (*23*, *33*) indicate that this complex does not produce APS and $PP_i$. Thus, isomerization precedes GTP hydrolysis, which, in turn, precedes α,*β*-bond scission. Given this ordering of events, the apparent simultaneous cleavage of the α,*β* and *β*,*γ* bonds can be explained on the basis of a rate-limiting isomerization followed by rapid GTP hydrolysis followed, in turn, by an even faster cleavage of the α,*β* bond. Simulations suggest that each successive step must be nominally ~6-fold of that of its antecedent for the reaction rates to appear identical. A consistent but unlikely alternative to the sequential-cleavage model is that the cleavages are in fact simultaneous; they are part of the same event and governed by a single rate constant. This model, which seems to place unreasonably stringent demands on synchronization of the bond cleavages, raises the issue of whether these three apparently simultaneous events (isomerization, *β*,*γ*-, and α,*β*-bond cleavages) are better viewed as a near continuum of interdependent molecular changes or as well-separated, consecutive events.

GDP activates APS synthesis far more weakly than GTP (*24*) and cannot elicit detectible isomerization from the enzyme; the allosteric network that activates APS synthesis is essentially inaccessible to GDP. Given that hydrolysis precedes α,*β*-bond cleavage, it appears that the α,*β*-bond must be both activated and cleaved by the ATP·$SO_4$·E·GDP·$P_i$ complex; this is supported by the observation than APS departs from the central complex far more rapidly that either GDP or $P_i$ (see *APS Is the First Product to Depart*, below). Generalizing, the function(s) of the E·GDP·$P_i$ complex of the ATP sulfurylase GTPase are distinct from those of the E·GDP form(s). Given that the cellular concentration of $P_i$ is comparable to its affinity constant for binding to the E·GDP forms of this and other GTPase (*24*), it is expected that the E·GDP·$P_i$ complexes of other GTPases, which have not been studied extensively, will be prevalent in the cell and exhibit distinct and perhaps important biological functions.

*Product Release.* Quenched-flow experiments typically measure the total product formed in a reaction and do not, therefore, distinguish between the enzyme-bound and solution-phase products. Consequently, if a product burst is observed, such measurements cannot identify which of the products is released slowly, causing the burst, or whether the release of products is ordered. Such distinctions *are* possible if solution-phase product formation can be monitored during the first turnover of the reaction. If, for example, release of one of two products is rate-limiting, its accumulation in solution will exhibit a lag because of the accumulation of that same product on the surface of the enzyme (i.e., the burst). The product whose release is not rate-limiting will exhibit a shorter lag, and the difference between the lags is indicative of the degree to which a particular order of release is preferred. Subtracting the concentrations of the solution-phase and total product yields the concentration of enzyme-bound product, which can be used in conjunction with $k_{cat}$ to obtain the rate constant governing the release of the product. The steady-state rate of reaction, $k_{cat} \times$ [active sites], must equal the release rate constant, $k_{release}$, times the concentration of the complex that delivers that product into solution (i.e., $k_{cat} \times$ [active sites] $= k_{release} \times$ [product complex]). In cases where multiple enzyme-bound forms of a product deliver the product into a solution, it may not be possible to assign release rate constants to each complex; rather, a composite or "net" constant is obtained.

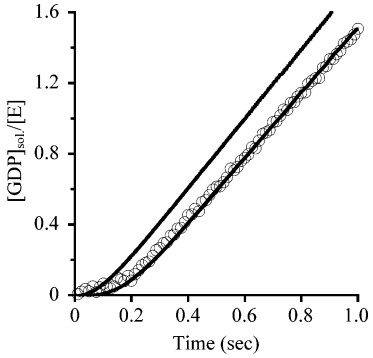


FIGURE 2: Solution-phase GDP in the early stages of the reaction. A solution containing NADH (200 $\mu$M), PEP (4.0 mM), GTP (4.0 mM), $MgCl_2$ (6.0 mM), $Na_2SO_4$ (2.0 mM), ATP (2.8 mM), $PP_i$ase (1.1 $\mu$M), PK (360 $\mu$M), LDH (120 $\mu$M), and Hepes (50 mM, pH 8.0) was mixed with a solution of equal volume containing ATP sulfurylase (20 $\mu$M), $MgCl_2$ (3.0 mM), and Hepes (50 mM, pH 8.0) in a stopped flow apparatus. Solution-phase GDP was monitored, using a stopped-flow fluorimeter, by coupling (1:1) its formation to the reduction of NADH using the coupling enzymes PK and LDH. The reactant solutions and equipment were equilibrated at 25 ± 2 °C prior to mixing. Additional details are described in *Materials and Methods*. The curve through the data represents the best fit of the data to a minimal mechanism in which the release of $P_i$ and $PP_i$ are ordered, with $P_i$ releasing first (see Figure 7 and *Modeling*). The curve rising above the data is an attempt to fit the data using a mechanism in which the $P_i$ and $PP_i$ release is random (see text).

*The Release of GDP.* GDP release was monitored with a stopped-flow apparatus using the fluorescence change associated with the oxidation of NADH, which was stoichiometrically (1:1) coupled to GDP production using PK and LDH. ATP sulfurylase was mixed in an equal volume with ATP (2.0 mM, 125 × $K_m$), $SO_4$ (2.8 mM, 67 × $K_m$) and GTP (4.0 mM, 630 × $K_m$) (see the caption of Figure 2 for further details). Under these conditions, GDP release exhibits a pronounced (~200 ms) lag (Figure 2) that is comparable in duration to the GDP burst shown in Figure 1. $k_{cat}$, calculated from the steady-state region of the curve, is 1.8 ± 0.05 $s^{-1}$, which is in excellent agreement with the numbers obtained from measurements performed at catalytic concentrations of the enzyme. Coupled reactions have intrinsic lags because of the fact that the product of the primary enzyme

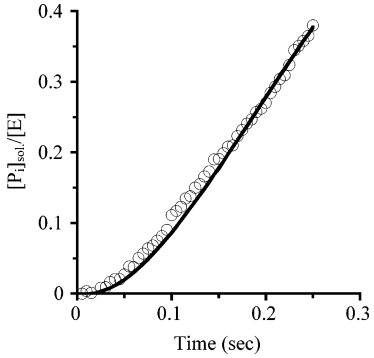


FIGURE 3: Solution-phase $P_i$ in the early stages of the reaction. The presence of phosphate in solution was detected by monitoring the fluorescence change associated with its binding to PBP. A solution containing PBP (40 $\mu$M), ATP (2.0 mM), GTP (4.0 mM), PEP (2.0 mM), $MgCl_2$ (3.0 mM), $Na_2SO_4$ (2.0 mM), PNP [0.04 unit (U)/mL], 7-methylguanosine (1.0 mM), and Hepes (50 mM, pH 8.0) was mixed rapidly using a stopped-flow fluorimeter with an equal volume of solution containing ATP sulfurylase (40 $\mu$M), PK (5.7 $\mu$M), $MgCl_2$ (3.0 mM), PNP (0.04 U/mL), 7-methylguanosine (1.0 mM), and Hepes (50 mM, pH 8.0) in the stopped-flow apparatus. The equipment and reagents were equilibrated at $25 \pm 2$ °C. Further details are described in *Materials and Methods*. The smooth curve is the best fit of the data obtained using the minimal model shown in Figure 7 (see *Modeling*).

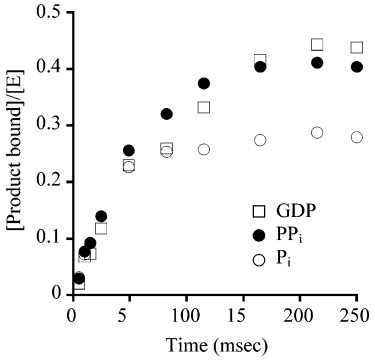


FIGURE 4: Enzyme-bound product concentrations in the early stages of the reaction. The progress curves for the formation of enzyme-bound GDP (□), $P_i$ (○), and $PP_i$ (●) were obtained by subtracting the solution-phase from the total-product data.

(ATP sulfurylase) must reach a concentration where the velocities of the coupled and primary reactions become equal, the steady state. To avoid artifacts, the intrinsic lag, which is a function of *V*/*K* (*34*−*37*), must be short compared to the lag associated with the primary enzyme. *V*/*K* values of the coupling enzymes were adjusted to achieve a suitable condition. The lag of the coupling system was determined experimentally by replacing ATP sulfurylase with guanylate kinase at a concentration that produced GDP at the same rate as ATP sulfurylase ($1.8 \pm 0.05$ $s^{-1}$) but was too small to produce a detectible lag from its own pre-steady-state behavior; thus, the observed lag is associated solely with the coupling system. The intrinsic lag, characterized previously and confirmed in the present work, is <30 ms (*18*).

*The Release of $P_i$.* Phosphate release was monitored continuously during the first ~2 turnovers of ATP sulfurylase using the fluorescently tagged phosphate-binding protein system developed by Webb *et al.* (*19*, *38*) (see Figure 3). Under the conditions of the current studies, this system undergoes a 3.8-fold change in fluorescent intensity upon binding phosphate and its intrinsic lag is quite short, ≤3 ms. Phosphate release exhibits a lag, ~40 ms, which is 5-fold shorter than that for GDP. Clearly, $P_i$ does not need to wait for the release of GDP to exit from the enzyme; its release either precedes or is concomitant with release of GDP.

*Enzyme-Bound Product Prior to and During the Steady State.* The time dependence of the bound product concentrations in the early stages of reaction are calculated by subtracting the solution-phase from total-product concentrations. Such subtractions (see Figure 4) reveal that bound $P_i$ (○), GDP (□), and $PP_i$ (●) (discussed below) accumulate at comparable rates in the very early stages of the reaction and that these progress curves separate as the system proceeds into the steady state. Bound $P_i$ plateaus earlier and at a lower level (~0.29 active-site equivalents) than either bound GDP (0.45) or $PP_i$ (0.41). The early, low E·$P_i$ plateau indicates either that $P_i$ is released faster than or prior to the release of GDP and/or $PP_i$. In the case of ordered release, the release rate constant does not need to be greater than that of the other substrates to observe an earlier and lower plateau.

Random and ordered mechanisms predict different net-rate constants for the release of $P_i$, GDP, and $PP_i$. The constants are calculated by dividing $k_{cat}$ by the fraction of the enzyme capable of releasing a particular product in the steady state. Assuming a random mechanism, the net-rate constants for release of $P_i$, GDP, and $PP_i$ are 6.1 $s^{-1}$ ($k_{cat}$/(fraction E bound to $P_i$) = 1.77 $s^{-1}$/0.29), 3.9 $s^{-1}$ (1.77 $s^{-1}$/0.45), and 4.3 $s^{-1}$ (1.77 $s^{-1}$/0.41), respectively. If one considers an ordered mechanism with $P_i$ departing first, the $P_i$ release rate constant is again 6.1 $s^{-1}$; however, the constants for release of GDP and $PP_i$ are calculated differently because only those product complexes without phosphate are capable of releasing these products. Thus, the net-rate constant for GDP release, 11 $s^{-1}$, is given by the expression: $k_{cat}$/(fraction of enzyme capable of releasing GDP) = 1.77 $s^{-1}$/(0.45−0.29); the denominator yields the fraction of the enzyme that contains GDP but not $P_i$. Similarly, the net-rate constant for release of $PP_i$ is 14 $s^{-1}$ = 1.77 $s^{-1}$/(0.41−0.29).

These mechanism-dependent sets of constants can be used to assess which mechanism is operative by comparing how well they predict experimental outcomes. Such a comparison is shown in Figure 2 in which the accumulation of solution GDP is simulated using random and ordered models in which the release rate constants were set equal to the values calculated for these mechanisms (preceding paragraph). The solid line that passes through essentially all of the data points is the behavior predicted using the ordered release mechanism; the line lying significantly above the data is the result predicted by the random mechanism. The reason that the random mechanism simulation is offset from the experimental data is that the mechanism predicts a lag that is too short to fit the data well. When two products are released randomly, they are released simultaneously into solution in accordance with the rate constants that govern their release. If, on the other hand, release is ordered, the lag phase for release of the second product is longer because its release initiates only after departure of the first product. Thus, sequential release produces a longer lag for the release of the second product, as is seen in the $P_i$ and GDP release data, where the lags are approximately 40 and 200 ms, respectively.

*Coupling-Enzyme (CE) Titrations Determine the Steady-State Distribution of the Enzyme.* Detection systems rapid enough to accurately report solution-phase and enzyme-bound product concentrations during the first turnover are not always accessible, such is the case with APS. To address this situation, a method that requires only a single CE (rather than a series of enzymes, each of which has a lag) was developed. As CE is titrated into a solution containing a fixed concentration of the primary enzyme (ATP sulfurylase) in steady-state turnover, the solution concentration of the primary product decreases and ultimately tends toward 0 as the ratio of the catalytic efficiencies of the two enzymes $((V_m/K_m)_{CE}/(V_m/K_m)_{ATP\ sulfurylase})$ approaches infinity. If a measurable quantity of the primary product remains bound to the surface of the enzyme during turnover, it will be inaccessible to the coupling enzyme and a plot of [product] versus [CE] will plateau, rather than approach 0, as the solution-phase product becomes negligible compared to that bound to the enzyme.

The CE-titration method was tested by comparing the steady-state concentration of enzyme-bound GDP determined using the CE method with the value obtained using the subtraction technique described above (Figure 5A). A solution containing ATP sulfurylase and PK (variable concentration) was mixed rapidly with a solution of equal volume containing [α-$^{32}$P]GTP, ATP, and $SO_4$ (at saturation after mixing) and coupling enzymes ($PP_i$ase and APS kinase) to prevent product inhibition (see the caption of Figure 5). The reactions produced ~1.9 active-site equivalents of product (1.0 s) before quenching, and radiolabeled reactants were separated using TLC chromatography and quantitated. The concentration of radiolabeled GDP descends, as a function of the increasing PK concentration, to a plateau at 0.47 enzyme equivalents, a value quite similar to that obtained using the subtraction approach, 0.45. The coincidence of these values validates the CE-titration method, and the CE-titration experiment verifies that the [CE] used in the continuous-monitoring experiments reduces the solution-phase product concentration sufficiently to reveal the enzyme-bound species.

*APS Departs First.* Continuous monitoring of solution-phase APS can be accomplished using APS kinase, PK, and LDH; however, the intrinsic lag associated with this string of three enzymes is too long to accurately report the solution concentration in the single-turnover regime. For this reason, a CE-titration experiment was performed using APS kinase, an extremely efficient enzyme [$k_{cat}/K_{m\ (APS)} > 10^8\ M^{-1}\ s^{-1}$ (*39*)]. The details of this experiment are identical to those associated with the GDP experiment described above, except that APS kinase, rather than PK, is the titrant, the labeled substrate is [γ-$^{32}$P]ATP, and the coupling enzymes present to prevent product inhibition are PK and $PP_i$ase. The result (Figure 5B) indicates that very little (2.0 ± 0.1%) of the enzyme is bound to APS in the steady state. Using the concentration of enzyme-bound APS and $k_{cat}$, the net-rate constant for APS desorbtion is calculated at 88 $s^{-1}$, a value considerably larger than that for GDP (11 $s^{-1}$), $P_i$ (6.1 $s^{-1}$), or, as is shown below, $PP_i$. The relatively quick departure of APS means that it leaves primarily from the quintinary ($GDP{\cdot}P_i{\cdot}E{\cdot}APS{\cdot}PP_i$) complex and that its departure initiates either before (ordered release) or is concomitant with (random release) departure of the other products. The rapid release of APS simplifies interpretation of the release of the other products because, as a result of their relatively slow departure, they will exit primarily from complexes that do not contain APS.

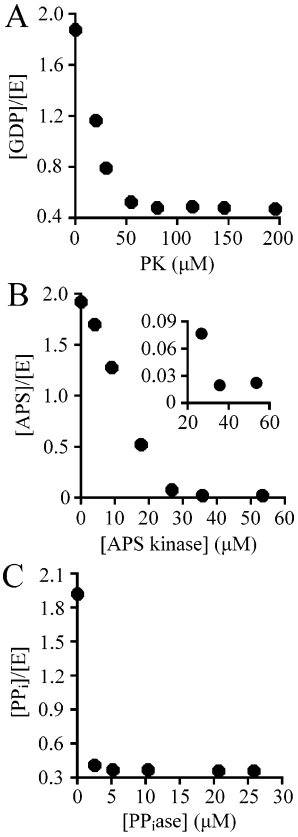


FIGURE 5: Coupling enzyme titrations provide the steady-state concentrations of enzyme-bound products. (A) Enzyme-bound GDP. A solution containing [α-$^{32}$P]GTP (518 μM, SA = 38 μCi/mL), ATP (1.0 mM), $Na_2SO_4$ (1.0 mM), $MgCl_2$ (3.0 mM), PEP (2.0 mM), APS kinase (106 μM), $PP_i$ase (54 μM), $MgCl_2$ (3.0 mM), and 50 mM Hepes (pH 8.0) was mixed rapidly using a quenched-flow apparatus with a solution of equal volume containing ATP sulfurylase (40 μM), $MgCl_2$ (3.0 mM), a varying concentration of PK, and 50 mM Hepes (pH 8.0). The reaction was allowed to proceed for a period of 1.00 s (1.7 turnover) before rapidly mixing with a quenching solution containing 150 mM EDTA/NaOH at pH 10.0. The solutions were equilibrated at 25 ± 2 °C prior to mixing. Radiolabeled reactants were separated, using TLC sheets, and quantitated (see *Materials and Methods*). Each point represents the average of three separate determinations. (B) Enzyme-bound APS. The experimental design was identical to that described in A, except that the APS kinase was the coupling-enzyme titrant and $SO_4$ (0.50 mM) was radiolabeled with $^{35}$S (SA = 42 μCi/mL). (C) Enzyme-bound $PP_i$. The experimental design was identical to that described in A, except that the $PP_i$ase was used as the coupling-enzyme titrant and ATP (0.50 mM) was γ-$^{32}$P-labeled (SA = 60 μCi/mL).

*The Release of $PP_i$.* Pyrophosphate release was studied using both the CE titration and continuous detection methods. The conditions of the CE titration were identical to the two previously described titrations, except that ATP is radiolabeled (γ-$^{32}$P), $PP_i$ase is the titrant, and the coupling enzymes added to prevent product inhibition are PK and APS kinase. The titration plateaus at 0.37 active-site equivalents (Figure 5C), which is comparable to the value of 0.41 observed using the subtraction method.

To gain further insight into the $PP_i$-release mechanism, inorganic pyrophosphatase [an extremely efficient enzyme, $k_{cat}/K_m \sim 2 \times 10^8\ M^{-1}\ s^{-1}$ (*40*)] and the PBP system were

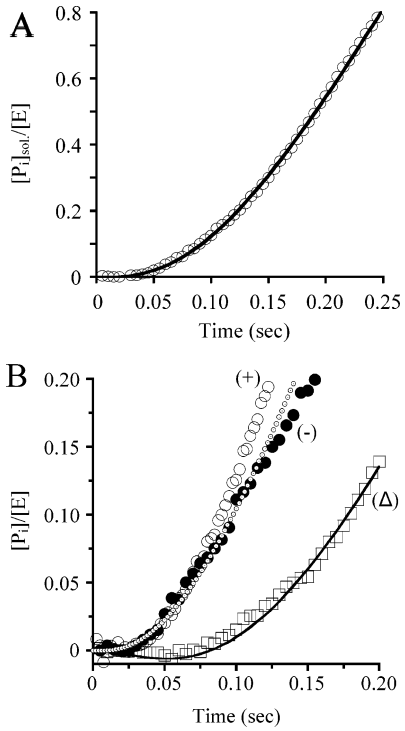


FIGURE 6: Solution-phase $P_i$ in the presence of $PP_i$ase. The terphosphate progress curve. In the presence of $PP_i$ase, three phosphates are produced per catalytic cycle by the hydrolysis of both GTP and $PP_i$. (A) Terphosphate release. Solution-phase phosphate was detected using PBP. The experimental conditions were identical to those associated with Figure 3, except that $PP_i$ase was added, at 30 $\mu$M, to the syringe containing ATP sulfurylase. The smooth curve is the behavior predicted by the best-fit parameters obtained by fitting the data with the minimal kinetic scheme shown in Figure 7 (see *Modeling*). (B) Solution-phase $PP_i$. The solution-phase $P_i$ data (●) [i.e., (−)-$PP_i$ase data] shown in Figure 3, was subtracted from the terphosphate data (○) [i.e., (+)-$PP_i$ase data] to yield the difference curve (□) (i.e., Δ data), which reports on solution-phase $PP_i$. The (+) and (−) curves are nearly identical until $PP_i$ first begins to appear in solution at ∼70 ms. The small open circles represent the best fit to the difference data (Δ) obtained using a mechanism in which $P_i$ and $PP_i$ are released randomly. The smooth curve passing through the Δ data is the behavior predicted by the best-fit parameters obtained by fitting the data with a minimal kinetic scheme in which the release of $P_i$ and $PP_i$ are ordered, with $P_i$ departing first (see Figure 7 and *Modeling*).

used together to continuously monitor $PP_i$ release. In the steady state, three $P_i$ will be released per turnover, one from the hydrolysis of GTP and the remainder from $PP_i$ hydrolysis. The conditions of the $PP_i$- and $P_i$-release experiments were identical except for the addition of $PP_i$ase. The pre-steady-state production of solution-phase $P_i$ in the presence of $PP_i$ase is shown in Figure 6A. $k_{cat}$, calculated from the steady-state region of the curve, is 1.7 (± 0.1) $s^{-1}$.

The terphosphate release progress curve was corrected to reveal the underlying release of $PP_i$ by subtracting the $P_i$ produced by GTP hydrolysis [i.e., the (−) $PP_i$ase data]. The signal-to-noise ratio of the datasets was high enough to yield a high-quality subtraction progress curve, the Δ curve, that reports exclusively on $PP_i$ release (Figure 6B). An expanded view of the early regions of the (+) $PP_i$ase, (−) $PP_i$ase, and Δ curves are shown in Figure 6B. The (+) and (−) curves are virtually identical during the first ∼70 ms and begin to separate just as the $PP_i$ (Δ curve) begins to appear in solution. As discussed above, if $PP_i$ and $P_i$ were released randomly,

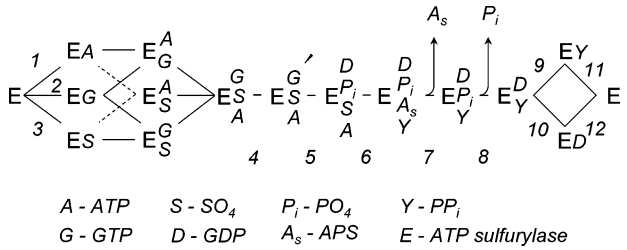


FIGURE 7: Minimal kinetic model. This model was used to generate all of the fits shown in the paper. Table 1 lists the rate constants obtained by simultaneously fitting the model to five different reactant time courses (see *Modeling* for further discussion).

$PP_i$ would appear concomitantly with $P_i$ in solution. This is not observed. Instead, the Δ curve remains essentially flat for ∼75 ms, ∼45 ms longer than the flat region of the (−) curve. Thus, $PP_i$ does not depart from the E·GDP·$P_i$·$PP_i$ complex until some other event occurs. As was the case with the release of GDP and $P_i$, the progress curve for solution-phase $PP_i$ is not well-fit using a mechanism in which $P_i$ and $PP_i$ are released randomly, because the lag for $PP_i$ release is too short using this mechanism (see small open circles in Figure 6B). However, the data are quite well-fit using an ordered mechanism in which $P_i$ is released first.

The implications of the ordering of events between the two chemistries are considerable. Obligate linking or ordering of the chemistries at any point in the mechanism will couple their Gibbs potentials. Thus, in addition to linking APS synthesis and GTP hydrolysis at the isomerization and bond-cleavage steps, the mechanism of ATP sulfurylase further links the chemical potentials at the product-release stage of the catalytic cycle.

*Modeling.* This paper presents five experimentally independent, time-course datasets that were used to develop a minimal model of the mechanism, the two burst datasets ($\alpha,\beta$ and $\beta,\gamma$ cleavage) and the three solution-phase product datasets (GDP, $P_i$, and terphosphate). In addition, the net-rate constants obtained from the CE titrations (also independent) were used to limit rate-constant ranges used in the model. The simplest model capable of fitting all of the data well was fashioned using rationales and data presented here and in previous publications and is presented in Figure 7. From left to right, the model proceeds from the random binding of substrates through an isomerization, a single bond-breaking step (which could be substituted by two steps whose overall character resembled that of the single step), the ordered release of APS, $P_i$, and the random release of GDP and $PP_i$. The ability of the model to predict the catalytic behavior of the enzyme was assessed by testing its ability to fit simultaneously the five independent experimental datasets. The test dataset was constructed by selecting the 13 data points associated with the time intervals used in the burst experiments from each of the five datasets. The resulting 85 data-point set was fit, with the Gepasi (*41*) program configured to use the Levenberg−Marquadt alogrithm. The resulting fit (the *core fit*) was quite good (SD = 0.092), and the resulting rate constants are compiled in Table 1 alongside their experimentally determined counterparts; the core-fit and experimental values agree well. The fits were further refined by fitting each dataset individually while allowing the core constants (with the exception of the substrate-binding constants) to vary by no more that 15%.

Table 1: Modeled and Experimental Rate Constants

| step[a] | forward / reverse | modeled | experimental |
|---|---|---|---|
| 1 | + | $3.4 \times 10^5$ $M^{-1}$ $s^{-1}$ | $3.4 \times 10^5$ $M^{-1}$ $s^{-1}$ |
| | − | 17 $s^{-1}$ | 17 $s^{-1}$ |
| 2 | + | $1 \times 10^6$ $M^{-1}$ $s^{-1}$ [b] | − |
| | − | 16 $s^{-1}$ | − |
| 3 | + | $1 \times 10^6$ $M^{-1}$ $s^{-1}$ [b] | − |
| | − | 42 $s^{-1}$ | − |
| 4 | + | 4.3 $s^{-1}$ | 2.5 $s^{-1}$ |
| | − | 1.2 $s^{-1}$ | 1.2 $s^{-1}$ |
| 5[c] | + | > 500 $s^{-1}$ | > 150 $s^{-1}$ [d] |
| 6[c] | − | < 1 $s^{-1}$ | − |
| 7 | + | 86 $s^{-1}$ | 89 $s^{-1}$ [f] |
| | − | ~ 0 [e] | − |
| 8 | + | 6.9 $s^{-1}$ | 6.1 $s^{-1}$ [f] |
| | − | ~ 0 [e] | − |
| 9 | + | 12 $s^{-1}$ | 11 $s^{-1}$ [f] |
| | − | ~ 0 [e] | − |
| 10 | + | 18 $s^{-1}$ | 14 – 25 $s^{-1}$ [f] |
| | − | ~ 0 [e] | − |
| 11 | + | 11 $s^{-1}$ | 14 – 25 $s^{-1}$ [f] |
| | − | ~ 0 [e] | − |
| 12 | + | 6.8 $s^{-1}$ | 11 $s^{-1}$ [f] |
| | − | ~ 0 [e] | − |

[a] Step numbers refer to the modeled mechanism in Figure 7. [b] Hypothetical on-rate constant; $k_-/k_+$ was set equal to $K_m$. [c] The bond-breaking steps, 5 and 6, were modeled as a single constant. [d] Determined using the E·AMP·$PP_i$ analogue complex. [e] Product off-rate steps were modeled as irreversible. [f] Net-rate constant for product release.

This procedure provides the model with a limited flexibility around the core, allowing it to better accommodate small deterministic errors between data sets. In this way, the nuances of the model can be assessed for their goodness-of-fit. The results of the refinements were satisfactory and are shown as solid lines passing through the data in all of the figures.

## CONCLUSIONS

The primary finding of this paper is that the chemical potentials of the chemistries catalyzed by ATP sulfurylase are coupled at multiple points along the reaction coordinate. The enzyme uses ordering of the catalytic events to interdigitate the chemistries, thereby harnessing their potentials to one another. Underlying the ordering of events is an allosteric communication between the active sites that dictates when and where a given event can occur in the catalytic cycle; arrival of the system at a particular point establishes contacts that initiate a molecular change that propagates to the distal site, enabling the reaction there to proceed to its next stage, whereupon signals may transit back to the original site, reporting that the distal event has occurred.

The tools developed here and in previous work, which may be of general value, have identified coupling events stretching from points in the catalytic cycle prior to chemistry through to steps involved in product release. The multiple, rich nature of the coupling in this system suggests that the mechanism might well contain additional coupling elements that are transparent to our current methodologies.

## REFERENCES


1. Siegel, L. M. (1975) Metabolism of sulfur compounds (Greenberg, D. M., Ed.) pp 217−286, Academic Press, New York.
2. Singleton, R. (1993) The sulfate reducing bacteria: An overview (Singleton, R., and Odom, J. M., Eds.) pp 1−20, Springer-Verlag, New York.
3. Mitchell, S. (1996) Biological interactions of sulfur compounds (Mitchell, S. C., Ed.) pp 20−41, Taylor and Francis, London, U.K.
4. Leyh, T. S. (1993) The physical biochemistry and molecular genetics of sulfate activation, *Crit. Rev. Biochem. Mol. Biol. 28*, 515−542.
5. Hiltz, H., and Lipmann, F. (1955) The enzymatic activation of sulfate, *Proc. Natl. Acad. Sci. U.S.A. 41*, 880−890.
6. Robbins, P. W., and Lipmann, F. (1958) Enzymatic synthesis of adenosine-5′-phosphosulfate, *J. Biol. Chem. 233*, 686−690.
7. Moore, K. L. (2003) The biology and enzymology of protein tyrosine O-sulfation, *J. Biol. Chem. 278*, 24243−24246.
8. Strott, C. A. (2002) Sulfonation and molecular action, *Endocr. Rev. 23*, 703−32.
9. Chapman, E., Best, M. D., Hanson, S. R., and Wong, C. H. (2004) Sulfotransferases: Structure, mechanism, biological activity, inhibition, and synthetic utility, *Angew. Chem. Int. Ed. 43*, 3526−3548.
10. Peck, H. D. J. (1993) The sulfate reducing bacteria: An overview (Singleton, R., and Odom, J. M., Eds.) pp 41−76, Springer-Verlag, New York.
11. Leyh, T. S., Taylor, J. C., and Markham, G. D. (1988) The sulfate activation locus of *Escherichia coli K*-12: Cloning, genetic, and enzymatic characterization, *J. Biol. Chem. 263*, 2409−2416.
12. Leyh, T. S., Vogt, T. F., and Suo, Y. (1992) The DNA sequence of the sulfate activation locus from *Escherichia coli K*-12, *J. Biol. Chem. 267*, 10405−10410.
13. Leyh, T. S., and Suo, Y. (1992) GTPase-mediated activation of ATP sulfurylase, *J. Biol. Chem. 267*, 542−545.
14. Wei, J., and Leyh, T. S. (1999) Isomerization couples chemistry in the ATP sulfurylase−GTPase system, *Biochemistry 38*, 6311−6316.
15. Foster, B. A., Thomas, S. M., Mahr, J. A., Renosto, F., Patel, H. C., and Segel, I. H. (1994) Cloning and sequencing of ATP sulfurylase from *Penicillium chrysogenum*. Identification of a likely allosteric domain, *J. Biol. Chem. 269*, 19777−19786.
16. Haldane, J. S. B. (1965) *Enzymes*, MIT Press, Cambridge, MA.
17. Wei, J., Tang, Q. X., Varlamova, O., Roche, C., Lee, R., and Leyh, T. S. (2002) Cysteine biosynthetic enzymes are the pieces of a metabolic energy pump, *Biochemistry 41*, 8493−8498.
18. Sukal, S., and Leyh, T. S. (2001) Product release during the first turnover of the ATP sulfurylase−GTPase, *Biochemistry 40*, 15009−15016.
19. Brune, M., Hunter, J. L., Howell, S. A., Martin, S. R., Hazlett, T. L., Corrie, J. E., and Webb, M. R. (1998) Mechanism of inorganic phosphate interaction with phosphate binding protein from *Escherichia coli*, *Biochemistry 37*, 10370−10380.
20. Wei, J., and Leyh, T. S. (1998) Conformational change rate-limits GTP hydrolysis: The mechanism of the ATP sulfurylase−GTPase, *Biochemistry 37*, 17163−17169.
21. Randerath, K., and Randerath, E. (1964) Ion-exchange chromatography of nucleotides on poly-(ethyleneimine)-cellulose thin layers, *J. Chromatogr. 16*, 111−125.
22. Bochner, B. R., and Ames, B. N. (1982) Complete analysis of cellular nucleotides by two-dimensional thin-layer chromatography, *J. Biol. Chem. 257*, 9759−9769.
23. Liu, C., Suo, Y., and Leyh, T. S. (1994) The energetic linkage of GTP hydrolysis and the synthesis of activated sulfate, *Biochemistry 33*, 7309−7314.

24. Liu, C., Wang, R., Varlamova, O., and Leyh, T. S. (1998) Regulating energy transfer in the ATP sulfurylase−GTPase system, *Biochemistry 37*, 3886−3892.
25. Leyh, T. S. (1999) On the advantages of imperfect energetic linkage, *Methods Enzymol. 308*, 48−70.
26. Wang, R., Liu, C., and Leyh, T. S. (1995) Allosteric regulation of the ATP sulfurylase associated GTPase, *Biochemistry 34*, 490−495.
27. Yang, M., and Leyh, T. S. (1997) Altering the reaction coordinate of the ATP sulfurylase−GTPase reaction, *Biochemistry 36*, 3270−3277.
28. Johnson, K. A. (1992) Transient-state kinetic analysis of enzyme reaction pathways, *Enzymes 20*, 1−61.
29. Admiraal, S. J., and Herschlag, D. (1995) Mapping the transition state for ATP hydrolysis: Implications for enzymatic catalysis, *Chem. Biol. 2*, 729−739.
30. Catrina, I. E., and Hengge, A. C. (2003) Comparisons of phosphorothioate with phosphate transfer reactions for a monoester, diester, and triester: Isotope effect studies, *J. Am. Chem. Soc. 125*, 7546−7552.
31. Guthrie, P. J. (1977) Hydration and dehydration of phosphoric acid derivatives: Free energies of formation of the pentacoordinate intermediates for phosphate ester hydrolysis and of monomeric metaphosphate, *J. Am. Chem. Soc. 99*, 3991−4001.
32. Wei, J., Liu, C., and Leyh, T. S. (2000) The role of enzyme isomerization in the native catalytic cycle of the ATP sulfurylase−GTPase system, *Biochemistry 39*, 4704−4710.
33. Liu, C., Martin, E., and Leyh, T. S. (1994) GTPase activation of ATP sulfurylase: The mechanism, *Biochemistry 33*, 2042−2047.
34. McClure, W. R. (1969) A kinetic analysis of coupled enzyme assays, *Biochemistry 8*, 2782−2786.
35. Cleland, W. W. (1979) Optimizing coupled enzyme assays, *Anal. Biochem. 99*, 142−145.
36. Easterby, J. S. (1973) Coupled enzyme assays: A general expression for the transient, *Biochim. Biophys. Acta 293*, 552−558.
37. Rudolph, F. B., Baugher, B. W., and Beissner, R. S. (1979) Techniques in coupled enzyme assays, *Methods Enzymol. 63*, 22−42.
38. Brune, M., Hunter, J. L., Corrie, J. E., and Webb, M. R. (1994) Direct, real-time measurement of rapid inorganic phosphate release using a novel fluorescent probe and its application to actomyosin subfragment 1 ATPase, *Biochemistry 33*, 8262−8271.
39. Satishchandran, C., and Markham, G. D. (1989) Adenosine-5′-phosphosulfate kinase from *Escherichia coli K*-12. Purification, characterization, and identification of a phosphorylated enzyme intermediate, *J. Biol. Chem. 264*, 15012−15021.
40. Belogurov, G. A., Fabrichniy, I. P., Pohjanjoki, P., Kasho, V. N., Lehtihuhta, E., Turkina, M. V., Cooperman, B. S., Goldman, A., Baykov, A. A., and Lahti, R. (2000) Catalytically important ionizations along the reaction pathway of yeast pyrophosphatase, *Biochemistry 39*, 13931−13938.
41. Mendes, P. (1997) Biochemistry by numbers: Simulation of biochemical pathways with Gepasi 3, *Trends Biochem. Sci. 22*, 361−363.

BI051303E